RESEARCH RESOURCE

Mouse redox histology using genetically encoded probes

Yuuta Fujikawa[1,2†], Leticia P. Roma[1†], Mirko C. Sobotta[1], Adam J. Rose[3], Mauricio Berriel Diaz[3,4], Giuseppe Locatelli[5], Michael O. Breckwoldt[5,6,7], Thomas Misgeld[6,8], Martin Kerschensteiner[5,8], Stephan Herzig[3,4], Karin Müller-Decker[9], & Tobias P. Dick[1*]

[1]Division of Redox Regulation, DKFZ-ZMBH Alliance, German Cancer Research Center (DKFZ), Im Neuenheimer Feld 280, 69120 Heidelberg, Germany. [2]Present address: School of Life Sciences, Tokyo University of Pharmacy and Life Sciences, 1432-1 Horinouchi, Hachioji, Tokyo 192-0392, Japan. [3]Joint Division Molecular Metabolic Control, DKFZ-ZMBH Alliance, German Cancer Research Center (DKFZ) Heidelberg, Center for Molecular Biology (ZMBH) and University Hospital, University of Heidelberg, 69120 Heidelberg, Germany. [4]Institute for Diabetes and Cancer (IDC) and Joint Heidelberg-IDC Translational Diabetes Program, Heidelberg University Hospital, Helmholtz Center Munich, 85764 Neuherberg, Germany. [5]Institute of Clinical Neuroimmunology, Ludwig-Maximilians Universität, 81377 Munich, Germany. [6]Institute of Neuronal Cell Biology, Technical University Munich and German Center for Neurodegenerative Diseases, 80802 Munich, Germany. [7]Present address: Department of Neuroradiology, University of Heidelberg, Im Neuenheimer Feld 400, 69120 Heidelberg, Germany. [8]Munich Cluster for Systems Neurology (SyNergy). [9]Core Facility Tumor Models, German Cancer Research Center (DKFZ), 69120 Heidelberg, Germany.

[†]equal contribution

*Corresponding author. E-mail: t.dick@dkfz.de

Mapping the in vivo distribution of endogenous oxidants in mouse tissues is of substantial biomedical interest. For example, it is of interest which particular organs, tissues, cell types and subcellular organelles exhibit redox changes in response to diet, exercise, disease or pharmacological intervention. Here we describe a procedure that conserves the in vivo redox state of genetically encoded redox biosensors within histological sections of mouse tissues, thus providing 'redox maps' for any tissue and comparison of interest. We demonstrate the utility of the technique by visualizing endogenous redox differences and changes in the context of tumor growth, inflammation, embryonic development and nutrient starvation.

INTRODUCTION

Endogenously produced reactive oxygen species are widely believed to play roles in health and disease. One species of particular interest is hydrogen peroxide (H_2O_2), which is traditionally implicated in 'oxidative stress', but is now known to play major roles in physiological signal transduction (*1*). Most intriguingly, H_2O_2 emitted from mitochondria may be a signal that links mild mitochondrial dysfunction (as it may occur during physical exercise or calorie restriction) to health benefits, through the induction of cytoprotective pathways, a concept now known as 'mitohormesis' (*2, 3*). The main mechanism by which H_2O_2 modulates cellular behavior is selective protein thiol oxidation, which in turn is antagonized by the NADPH-dependent thiol reducing systems. Glutathione (GSH) is the dominant low-molecular-weight thiol inside mammalian cells. Correspondingly, differences or changes in the degree of glutathione oxidation are commonly considered to indicate shifts in endogenous 'redox balance'. The recent development of genetically encoded fluorescent probes for H_2O_2 (*4, 5*) and for the glutathione redox potential (E_{GSH}) (*6*), represented a major advance, as it allowed to obtain subcellular compartment-specific real-time information from within living cells and whole organisms (*7, 8*). It is increasingly recognized that compartmental and chemical specificity are crucial for obtaining meaningful insights from redox measurements (*9, 10*).

Unfortunately, when expressed in multicellular organisms, the in vivo use of fluorescent proteins is fundamentally limited by optical accessibility. Consequently, transgenic redox

reporters have been used preferentially in small and/or translucent model animals (*7, 11, 12*). For mice, direct in vivo imaging is limited to superficial tissues or to those that can be made accessible by surgical intervention (*8*). It remains a major goal to make subcellular-resolution redox imaging generally applicable to mouse studies. It is important to realize that many fundamental questions can be addressed by analyzing mice at given time points, without the need for continuous real-time monitoring. For example, commonly encountered questions include whether genetic alterations, infections, ageing, exercise, changes in diet, toxins, or pharmacological treatments lead to redox changes in vivo. Most importantly, it is imperative to discover within which organs, tissues, cell types and subcellular organelles these changes occur. Hence, we were looking for a procedure that conserves and visualizes the endogenous state of genetically encoded redox probes in the context of histological tissue sections, thus providing sectional 'redox maps' for any organ or tissue of interest. This approach would necessarily be limited to providing 'snap shots' at selected time points, but in exchange should allow a comparison of the effect of any condition or treatment in almost any mouse model and in almost any tissue of interest with subcellular resolution.

In this paper, we present a straightforward procedure that allows conserving and visualizing the endogenous biosensor redox state within murine tissue sections. In this procedure initial cryogenic conservation is followed and replaced by chemical conservation to produce tissue sections in which biosensors maintain their endogenous redox state and resist artificial oxidation by atmospheric oxygen, fixatives or other influences. In short, the organ of interest is snap-frozen and cryosectioned. Cryosections are immediately immersed in *N*-ethyl maleimide (NEM), a fast-acting membrane-permeable alkylating agent, to clamp the in situ redox state of roGFP2 within the cryosection. Alkylation rapidly and irreversibly arrests reduced biosensor molecules in the reduced state, precluding ex vivo oxidation by atmospheric oxygen or paraformaldehyde (PFA) treatment, thus allowing for subsequent fixation and storage. We demonstrate that the succession of cryogenic and chemical preservation effectively prevents artificial probe oxidation and preserves reduced tissues in their reduced state. To explore the scope of the technique we introduced roGFP2-based redox probes into mice by three different means: tumor xenografting, adenoviral gene transfer and transgenesis. We provide examples for the detection of redox differences within normal and tumor tissues, for changes occurring during embryonic development and for changes caused by inflammation and nutrient starvation.

RESULTS

Redox imaging of xenografted tumors

To validate the cryogenic-chemical probe preservation technique (**Fig. 1A**), we first investigated a typical tumor xenograft model. A human non-small-cell lung cancer cell line (H1975) stably expressing mito-roGFP2-Orp1 (*4*), a mitochondrial H_2O_2 biosensor (mechanism shown in **Fig. 1B**), was established. Proper mitochondrial localization (**Fig. 2A**), dynamic responsiveness to either exogenous (**Fig. 2B**) or endogenous oxidants (**Fig. 2C**), and full protection against PFA-induced oxidation by NEM (**Fig. 2, D and E**) were confirmed in vitro on the cellular level. Corresponding tumors grown subcutaneously in athymic nude mice were snap frozen and cryosectioned. We confirmed that the probe within the cryosection exhibited its expected responsiveness and dynamic range (**fig. S1, A and B**). Using the NEM-based conservation protocol, we mapped the degree of probe oxidation over broad regions of the tumor mass (**Fig. 2F**). The necrotic core, identified by low nuclear density and standard HE-staining of serial sections, exhibited almost full roGFP2 oxidation, even though mitochondrial shape was retained. In the non-necrotic regions, the mito-roGFP2-Orp1 redox state was highly heterogeneous, ranging from almost completely reduced to fully oxidized (**Fig. 2G**). These differences may arise from clonal and/or metabolic heterogeneity within the tumor mass, possibly associated with differences in oxygen and/or nutrient availability. As expected, highly oxidized intratumoral regions remained oxidized regardless of NEM treatment, whilst intratumoral regions of lower oxidation showed artificial oxidation only in the absence of NEM treatment (**Fig. 2, H and I**). Thus, PFA-induced probe oxidation was completely prevented by NEM treatment of specimens.

Redox imaging following adenovirus-mediated probe transduction

Next, we used adenovirus-mediated gene transfer through tail vein injection to express the mito-roGFP2-Orp1 probe in the liver. Proper mitochondrial expression (**fig. S2A**), responsiveness and dynamic range (**fig. S2, B and C**), and effectiveness of redox state conservation by NEM treatment (**fig. S2, D and E**) were confirmed on liver tissue sections. To investigate the influence of liver inflammation on the mitochondrial redox state, we injected mice with either tumor necrosis factor alpha (TNFα), lipopolysaccharide (LPS) or concanavalin A (ConA). All three compounds produced heterogeneous effects, i.e. increased probe oxidation in a sparse population of cells (**Fig. 3, A and B; fig. S3, A and B**). To

demonstrate the possibility of combining redox probe measurements with conventional immunohistochemistry, we stained representative NEM-treated PFA-fixed sections with an antibody against complement receptor type 3 (CD11b). Regions of probe oxidation were found to co-localize with CD11b reactivity, implicating macrophages as a source of probe oxidation (**Fig. 3, C and D)**. These results further confirmed the ability of NEM-mediated probe conservation to reveal endogenous redox differences and changes, here in the context of inflammation.

Redox imaging of tissue sections from biosensor-transgenic mice

The above results suggested that the NEM-based conservation method can also be applied to analyze deep solid tissues from biosensor-transgenic mice. First, we made use of mice expressing a mitochondrial E_{GSH} probe (*6*) (mechanism shown in **Fig. 1C**) under a neuron-specific promoter (*Thy1*-mito-Grx1-roGFP2), as previously characterized and used by us for in vivo two-photon imaging of the spinal cord (*8*). After confirming the effectiveness of the probe conservation procedure in this system (**fig. S4, A-D**), we asked if endogenous local differences in E_{GSH} can be detected on brain sections. Ratiometric imaging of NEM-conserved hippocampus sections revealed that dentate gyrus granule cells (GcDG) are associated with a more reducing E_{GSH} than pyramidal cells (Py) in the cornu ammonis 1 (CA1) and 2/3 (CA2, CA3) regions (**Fig. 4, A-C; fig. S4E**).

Second, we generated mice expressing the H_2O_2 probe mito-roGFP2-Orp1(*4*) globally (*ROSA26*/CAG-stop^{fl}-mito-roGFP2-Orp1 x CMV-Cre). Again, we found that NEM conserved the status of highly reduced tissues (**Fig. 5, A and B**), and completely prevented any further oxidation within tissue sections (**Fig. 5C**). We first asked if regions of enhanced endogenous H_2O_2 generation can be detected in early embryos. The small diameter of early embryos allowed for a variation of the protocol in that whole embryos were treated sequentially with NEM and PFA, prior to cryosectioning. NEM-permeated E12.5 embryos revealed globular regions of increased probe oxidation in the liver (**Fig. 5D, fig. S5**). These regions likely represent clusters of proliferating and/or differentiating cells, as both hematopoietic stem cell differentiation and hepatocyte expansion are suggested to involve increased production of H_2O_2 (*13-15*). To further exemplify the use of NEM-permeated cryosections from mito-roGFP2-Orp1-transgenic mice we compared muscle tissues from fed and starved animals. Starvation was found to increase mitochondrial H_2O_2 probe oxidation (**Fig. 5, E and F**), in line with the observation of accelerated fatty acid oxidation (*16*), and with the suggestion that

starvation-induced oxidants trigger autophagy, thus leading to skeletal muscle atrophy during nutrient deprivation (*17*). Notably, oxidative and glycolytic muscular fibers (as differentiated by mitochondrial content) exhibited different probe redox states (**Fig. 5, G-H, fig. S6**).

DISCUSSION

The wide-spread application of genetically encoded fluorescent redox probes to mouse preclinical models has been substantially limited because most organs and tissues are not optically accessible in the living organism. Here, we show that a simple chemical conservation procedure can be combined with cryosectioning to reveal the spatial distribution of in vivo probe redox states on tissue sections from mice (or xenotransplantated tumors) expressing roGFP2-based redox probes. The chemical preservation step is based on the membrane-permeable thiol-alkylating agent N-ethyl maleimide (NEM) which combines several favorable properties. First, NEM by itself does not interfere with roGFP2 fluorescence measurements, neither in the unconjugated, nor in the thiol-conjugated state. Second, NEM protects the reduced probe against oxidation by irreversibly alkylating the roGFP2 cysteines. The ratiometric change in probe fluorescence upon oxidation is caused by the formation of a strained disulfide bond (*18*). Alkylation of the free cysteines by NEM thus locks roGFP2 in the strain-free state. Importantly, alkylation of the roGFP2 cysteines does not change the fluorescent properties of roGFP2. The alkylated and non-alkylated forms of reduced roGFP are indistinguishable on the basis of fluorescence (*6*). Likewise, the spectral properties of oxidized roGFP2 are not influenced by NEM. Third, NEM treatment additionally protects against reduction of oxidized roGFP because it generally alkylates free thiols, thus preventing fortuitous reduction of oxidized roGFP by disulfide exchange with thiols contained within the tissue section. Fourth, NEM penetrates tissues rapidly and efficiently, especially when applied to thin sections which are at most a few cell layers in diameter. The sections are alkylated instantly, due to short diffusion distances and simultaneous exposure to NEM from both sides. It should be clarified that the roGFP disulfide can still be reduced within the NEM-blocked section if a sufficiently large excess of reductant (e.g. DTT) is applied from outside. It will penetrate the section, consume any remaining free NEM, and then reduce any disulfide bonds (including those in roGFP). However, this is neither a concern, nor is it relevant to our procedure, because reductive equivalents will not emerge or be re-created within NEM-blocked tissue sections unless a reductant is deliberately applied from outside. Indeed, in our

hands NEM-blocked and fixed tissue sections do not show changes in roGFP2 signals when stored over prolonged periods of time.

We further show that roGFP2 fluorescence imaging can be combined with conventional immunohistochemistry, thus expanding the scope of the technique towards the identification of cell types associated with oxidative changes. In general, NEM treatment of tissue sections is not expected to interfere with antibody staining. Although, in principle, it is conceivable that a cysteine-containing epitope loses antibody affinity after being modified by NEM, such a situation would probably be exceptional and could be addressed by using alternative antibodies. Although we have only used mitochondrially targeted probes in this study, the procedure will equally apply to roGFP2-based probes targeted to other compartments (including the cytosol), as long as they provide a sufficient signal to noise ratio. A specific advantage of roGFP2-based probes is their ratiometric insensitivity to pH changes (*10*), which is a major drawback for any probe based on cpYFP (*19-21*). At present, chemical probes do not offer the combination of advantageous properties integral to genetically encoded probes. Moreover, in vivo applications of chemical probes suffer from pharmacokinetic constraints and may give rise to artifacts by tissue- or cell type-specific differences in uptake and/or export.

Limitations that generally apply to genetically encoded reporters also apply to the redox probes used in this study, as reviewed previously (*10, 22*). One potentially relevant limitation in the context of histological redox imaging is sensitivity. The H_2O_2-sensitive probe roGFP2-Orp1 is of similar sensitivity as the HyPer probe (*4*), but is less sensitive than peroxiredoxin-2, one of the most H_2O_2-sensitive proteins in mammalian cells (*23*). As shown here and elsewhere, many phenomena, related to both stress and signaling situations, can be sensed by the roGFP2-coupled Orp1 domain, a non-seleno glutathione peroxidase family member. Yet, detection of the slightest (metabolic) H_2O_2 fluctuations, close to the steady state baseline, probably taking place in the low nanomolar or even picomolar range, will probably require the development of peroxiredoxin-based redox probes. Peroxiredoxins are increasingly recognized to engage in redox relays (*24*) and therefore should also be able to communicate their redox state to roGFPs. In any case, the protocol described herein will also apply to future probes operating on the basis of roGFP.

In summary, the key advantages of genetically encoded redox probes, namely defined cellular and subcellular location, chemical specificity, and ratiometric measurement, are made available to a very broad range of histological studies. The chemical conservation approach

should be applicable to investigate the occurrence of redox differences and changes under various physiological and pathological conditions. For example, it is often suggested that most cancer cells exhibit increased endogenous ‘ROS’ generation, leading to either increased steady state levels or increased turnover of ‘ROS’. This has led to idea that drugs that further enhance ‘ROS’ generation (or selectively inhibit reducing systems) will push tumor cells over their tolerable threshold of ‘oxidative stress’, thus triggering selective cell death (*25*). However, in previous intervention studies it remained mostly unknown to which extent drugs actually reached different parts of a tumor, to which extent redox changes were actually inflicted in situ, and to which extent tumor cells responded differently relative to surrounding healthy tissues. Histological redox imaging should now allow to investigate more directly how tumors and their surroundings respond to pro-oxidative or anti-reductive drugs, alone or in combination with conventional radio- or chemotherapy. It may also be of interest to study the redox response of healthy and tumor tissues to ‘anti-oxidants’, given recent findings suggesting that compounds that are believed to act as ‘anti-oxidants’ can accelerate tumor progression and promote metastasis (*26-28*).

MATERIALS AND METHODS

Cell culture

Phoenix-Ampho and HEK293 cells were grown in Dulbecco's Modified Eagle Medium (DMEM) (Invitrogen, Karlsruhe, Germany). H1975 non-small-cell lung carcinoma cells (obtained from ATCC) were grown in RPMI1640 (Invitrogen). Media were supplemented with 10% heat-inactivated fetal bovine serum (Invitrogen), 2 mM L-glutamine (Invitrogen), 100 units/ml penicillin and 100 mg/ml streptomycin (Invitrogen). Cells were incubated in a humidified atmosphere of 5% CO_2/95% air at 37°C.

Stable expression of mito-roGFP2-Orp1 in H1975 cells

H1975 cells stably expressing mito-roGFP2-Orp1 were established by retroviral transduction. Briefly, Phoenix-Ampho cells were transfected with pLPCX/mito-roGFP2-Orp1 (encoding the roGFP2-Orp1 probe with an N-terminal mitochondrial targeting sequence) by the calcium phosphate method. After 6 h of transfection, cells were washed twice with PBS and transferred to fresh medium. After 24 and 48 h of transfection, supernatant was collected and passed through a 0.22 µm filter. H1975 cells (seeded at 2.7 x 10^5 cells/well in a 6 well plate for 24 h prior to each experiment) were incubated with the virus-containing supernatant supplemented with 4 µg/ml polybrene for 24 h at 37°C in a 5% CO_2 atmosphere. Cells were then grown in medium containing 0.5 µg/ml puromycin for several days. A highly fluorescent cell population (~6% of overall population) was selected by flow cytometry (FACS Aria). Collected cells were expanded in the medium containing 0.5 µg/ml puromycin and 50 µg/ml gentamycin.

Subcellular localization of mito-roGFP2-Orp1

Targeting of mito-roGFP2-Orp1 to mitochondria was confirmed by co-localization with TMRM (Molecular probes, Carlsbad, CA, USA). Cells placed in cell culture dishes (FluoroDish, World Precision Instruments, UK) were washed twice with Dulbecco's Phosphate Buffered Saline (DPBS) (Invitrogen) and incubated with TMRM in Hank's Buffered Salt Solution (HBSS) (Invitrogen) for 20 min at 37°C. roGFP2 fluorescence was excited with the 488 nm laser line and TMRM fluorescence with the 543 nm laser line on a Zeiss LSM 710 ConfoCor 3 microscope equipped with a Plan-Apochromat 63x/1.40 NA DIC oil immersion objective.

In vitro characterization of H1975/mito-roGFP2-Orp1 cells

4 x 10^4 H1975/mito-roGFP2-Orp1 cells in 400 µl of RPMI/10% FBS/25 mM HEPES were seeded into the wells of a Lab-Tek chamber slide (Fisher Scientific GmbH, Schwerte, Germany) one day prior to the experiment. Images were obtained with a Zeiss LSM 710 ConfoCor 3 microscope equipped with an EC Plan N DICI 40x/1.3 NA objective (oil immersion) and Zen software. roGFP2 fluorescence was excited sequentially at 405 nm and 488 nm (line by line) followed by detection of the emission through the 500–550 nm band-pass filter. Real-time measurements were conducted in time-series mode under 5% CO_2 and 37°C. After three 15 s intervals, 200 µl of medium containing the compound of interest (H_2O_2, rotenone, or antimycin A; at 2x final concentration) were added to the cells. Subsequent images were obtained every 15 s.

Animal experiments

Animal experiments were conducted according to local, national, and EU ethical guidelines and approved by local regulatory authorities.

Xenograft experiments

5 week old female NMRI (nu/nu) mice (Charles River Laboratories, Sulzfeld, Germany) were used for xenografting. After one week of acclimatization to individually ventilated cages, Kliba chow 3307 and water *ad libitum*, 5 x 10^6 H1975/mito-roGFP2-Orp1 cells were injected subcutaneously. Tumors were allowed to grow up to a size of 15 mm in one diameter, followed by embedding into TissueTEK OCT compound and snap freezing in isopentane/liquid nitrogen prior to storage at -80°C.

Preparation of recombinant adenovirus

Adenovirus expressing mito-roGFP2-Orp1 was generated using a modified pAd-BLOCK-iT vector system (Invitrogen, Karlsruhe, Germany). The mito-roGFP2-Orp1 coding sequence was subcloned into a pENTR™ entry vector modified to express the probe under control of the CMV promoter, followed by integration into pAd/Block-iT™ DEST. Adenoviruses expressing mito-roGFP2-Orp1 were produced using the BLOCK-iT adenoviral RNAi expression system (Invitrogen) according to the manufacturer's instructions and purified by cesium chloride gradient[29].

In vivo gene transfer and induction of liver inflammation

Male C57BL/6 mice (Charles River Laboratories, Brussels, BEL) were maintained on a 12 hour light-dark cycle with regular unrestricted diet. After one week, 2 x 10^9 plaque-forming units (pfu) of adenovirus were administered via tail vein injection. After another week, mice were subjected to the following treatments: intraperitoneal injection of 1 µg recombinant mouse TNFα (410-MT, R&D systems); 20 mg/kg lipopolysaccharide (055:B5) (L4524, Sigma-Aldrich, Munich, Germany), and intravenous injection of 40 mg/kg concanavalin A (L7647, Sigma-Aldrich). PBS was injected as vehicle treatment. Mice were sacrificed and analyzed 8 hours after the injection of inflammatory mediators.

Generation of transgenic mice

The generation of mice expressing mito-Grx1-roGFP2 under control of the *Thy1* promoter has been described previously(*8*). To generate mito-roGFP2-Orp1 expressing mice, roGFP2-Orp1 with a COX8 mitochondrial targeting sequence (*N. crassa*) was cloned into a modified version of the targeting vector pROSA26-1(*30*) (a kind gift from Dr. Marc Schmidt-Supprian) using AscI and SmaI restriction sites. The resulting targeting vector contains a CAG promoter, a loxP-flanked neo^r-stop cassette, the COX8-roGFP2-Orp1 construct and a polyadenylation sequence (pROSA26-CAG-loxP-Stop-loxP-AscI-COX8-roGFP2-Orp1-SmaI-polyA). Electroporated JM8.A3 ES cells(*31*) were selected with neomycin and positive clones were microinjected into C57BL/6N blastocysts and further processed as described by Pettitt and colleagues[(31)]. Chimeric mice were bred for homozygous transgene insertion, crossed with CMV-Cre mice, then selected for homozygous deletion of the stop cassette.

Preparation of murine tissue sections

Harvested tissues were embedded in Tissue-Tek OCT compound and snap frozen in isopentane/liquid nitrogen prior to storage at -80°C . Embedded tissues were warmed to -20°C (brain tissue) or to -25°C (other tissues), cryosectioned into 14 µm slices with a cryotome (Leica CM3050), and mounted onto SuperFrost Plus® slides (Fisher Scientific GmbH). Immediately after mounting, sections were subjected to chemical treatment. To induce maximal probe oxidation or reduction, sections were incubated for 10 min at 4°C with 50 µl PBS (10.1 mM $NaHPO_4$, 1.8 mM KH_2PO_4, 136.8 mM NaCl, 2.7 mM KCl) containing 1 mM diamide (DA) or 10 or 20 mM dithiothreithol (DTT), respectively. To conserve the

endogenous redox state, sections were immediately incubated with 80-100 µl PBS containing 50 mM NEM (Sigma-Aldrich, E3876) for 10 min at 4°C followed by fixation in 4% PFA in PBS containing 1 µM To-Pro-3 (using 0.1% DMSO as a co-solvent) (T3605, Invitrogen) for 15 min at ambient temperature. PFA was washed out twice with ice-cold PBS for 5 min. Sections were then mounted in Mowiol mounting medium (17% w/w Mowiol4-88 in PBS/Glycerol 2:1 (v/v)) and kept at 4°C until use.

Immunofluorescence

CD11b: Following fixation (4% PFA in PBS), sections were washed twice with ice-cold PBS for 5 min, and immediately incubated for 60 min in blocking buffer (5% normal goat serum (Cell Signaling, 5425) in PBS). Sections were subsequently incubated with an antibody against CD11b conjugated to Alexa Fluor 594 which was diluted (1:1500) in PBS with 1% BSA. Sections were incubated overnight at 4°C in a humid light-tight box. Sections were washed three times with PBS and mounted using Prolong® Gold Antifade Reagent (Cell Signaling, 8961). Microscopy images were taken within 24 hours.

MnSOD1: Livers were fixed overnight with 4% PFA immediately after excision. Sections (50 µm thickness) prepared by vibratome were rinsed three times with ice-cold PBS for 5 min and incubated for 60 min in blocking buffer (5% normal goat serum, 0.25% Triton X-100 in PBS) at room temperature. Sections were subsequently incubated with an antibody against MnSOD (Stressgen, ADI-SOD-110) in antibody dilution buffer (PBS containing 1% BSA and 0.25% Triton X-100) for 20 hours at 4°C. Sections were washed three times in PBS for 5 min and incubated in antibody dilution buffer with a secondary antibody against rabbit IgG conjugated to Alexa Fluor 594 (Invitrogen, A11012) (1:300) for 2 hours at room temperature in the dark. Sections were incubated in PBS containing 0.5 µM ToPro3 for 20 min, rinsed three times in PBS for 5 min, and mounted in Mowiol mounting medium.

Starvation

Mice were maintained on a 12-hour light/dark cycle in a temperature-controlled barrier facility, with free access to water and food. To examine the effects of fasting on biosensor oxidation, 12 week old female mice (mito-roGFP2-Orp1-expressing or control mice) were fasted for 22-24 hours or fed ad libidum. After this period, gastrocnemius/soleus muscles were dissected as fast as possible and embedded into Tissue-Tek OCT compound and snap frozen in isopentane/liquid nitrogen prior to storage at -80°C. Sections were processed as

described above, with minor modifications: Muscle sections were incubated with 50 µl PBS or PBS containing 50 mM NEM for 10 min at 4°C followed by fixation in 4% PFA in PBS for 30 min at room temperature. PFA was rinsed twice with ice-cold PBS for 10 min. Sections were then mounted in Mowiol mounting medium (17% w/w Mowiol4-88 in PBS/Glycerol 2:1 (v/v)) and kept at 4°C until use. Microscopy images were taken within 24 h after sectioning. Five-to-six animals, from three different preparations were used for each condition. Mice lacking biosensor expression (*ROSA26*/CAG-stop^{fl}-mito-roGFP2-Orp1 with intact stop cassette) were used as autofluorescence background controls.

Preparation of embryonic tissue sections

At embryonic day 12.5 (E12.5) embryos were collected, immediately immersed in PBS containing freshly dissolved NEM (100 mM) and incubated for 1.5 h at 4°C, followed by fixation in 4% PFA in PBS (pH 7.4) plus 100mM NEM for 1.5 h, at room temperature. Embryos were washed two times in PBS for 10 min and embedded in Tissue-Tek OCT compound and snap frozen in isopentane/liquid nitrogen prior to storage at -80°C. The embryos were oriented to obtain a longitudinal section of the whole animal. At the day of the experiment, the samples were removed from -80°C and kept at -20°C for one hour prior to sectioning. Sections of 14 µm thickness were cut by cryostat, mounted on SuperFrost Plus® slides (Fisher Scientific GmbH) and dried for 5 min at room temperature. Sections were then mounted in Mowiol mounting medium and kept at 4°C until use. Microscopy images were taken within 24 h after sectioning.

Image acquisition and image acquisition controls

Guidelines for the use of roGFP2-based redox probes, including microscopy settings and image analysis, have been provided previously (*32*, *33*). In general, fluorescence images were acquired frame-by-frame by measuring emission at 520-540 nm and exciting sequentially with the 405 nm and 488 nm laser lines. For each animal at least two images were taken from one or more sections. For starvation experiments images were acquired using a 40x objective. Tumor, coronal hippocampus, liver and embryo images were acquired with a 20x objective on a Leica TCS SP5 inverted confocal microscope using automated tile scanning with 10% overlap between individual images. In order to control for auto-fluorescence in tissue sections, we used two approaches: (i) control images were taken from tissues lacking biosensor expression (i.e. *ROSA26*/CAG-stop^{fl}-mito-roGFP2-Orp1 with intact stop cassette or non-

transduced). These tissues were treated in the same way and resulting images were used as general auto-fluorescence background controls. (ii) For every sample an image was acquired with excitation at 405 nm and emission at 460 nm. This image was used to set the lower threshold to a value above the background fluorescence. These controls were also applied to samples from the developing fetal liver to detect potential auto-fluorescence of developing blood cells, which however showed very weak fluorescence in all emission.

Image processing

In brief, raw image data of the 405 nm and 488 nm laser lines were exported to ImageJ as 16-bit TIFFs for further analysis. After conversion to 32-bit images, upper and lower thresholds were set for both images in order to remove background fluorescence and overexposed pixels. Ratio images were created by dividing the 405 nm image by the corresponding 488 nm image pixel by pixel. For visualization of the ratiometric images the ImageJ lookup table "Fire" was chosen. For additional quality control, representative images were subjected to detailed inspection and analysis as described previously for Drosophila tissues (*33*).

Data representation and statistics

Data are represented as either normalized fluorescence ratios (405/488 nm) or as degree of roGFP2 oxidation (OxD_{roGFP2}), as either box-whisker plot, dot plot, or bar chart. In most experiments, fully oxidized (diamide) and reduced (DTT) samples were prepared to allow calculation of the degree of probe oxidation. 405/488 nm raw ratio values were normalized by setting the oxidized state (diamide control) to 1 (i.e. $R_{norm} = (1/R_{ox})*R$) or converted to OxD values as previously described (*18*). In box-whisker plots, data are represented as median values with a box for the interquartile range and whiskers for the 5/95% percentiles. Bar diagrams represent normalized ratios as the mean $\pm$ S.E.M. In single cell analyses, 30 cells per sample were randomly collected as individual ROIs and measurements were represented as dot plot. The sample size (n) represents the number of samples used for statistics. Statistical comparison of multiple groups was done with Kaleida graph 4.1J (Synergy software) using ANOVA followed by non-parametric post-hoc Scheffe test. Student's t-test was used for binary comparisons. Statistical significance was defined as *p <0.05, ** p<0,01, ***p< 0.001.

FIGURE LEGENDS

Fig. 1. Probe conservation strategy and mechanisms of sensing. (**A**) Cryopreserved organs are cryosectioned and sections immediately treated with the fast-acting thiol blocker NEM to exclude artificial roGFP2 thiol oxidation during tissue fixation with PFA. (**B**) Mechanism of H_2O_2 sensing by roGPF2-Orp1. (**C**) Mechanism of GSSG sensing by Grx1-roGFP2.

Fig. 2. In situ visualization of the conserved in vivo roGFP2-Orp1 redox state on tumor tissue sections. (A) Colocalization of roGFP2 and tetramethylrhodamine (TMR) fluorescence in H1975 cells stably expressing mito-roGFP2-Orp1. Green: roGFP2; Red: TMR; White: colocalized pixels. Scale bar: 40 µm. **(B)** Response of H1975/mito-roGFP2-Orp1 cells to exogenously added H_2O_2. **(C)** Response of H1975/mito-roGFP2-Orp1 cells to endogenous H_2O_2 as induced by respiratory chain inhibitors rotenone and antimycin A, added 30 s after start of the measurement. **(D, E)** roGFP2 redox state upon PFA fixation . **(D)** NEM pretreated and fixed cells show a redox state comparable to NEM treated unfixed cells. Error bars represent S.D. of the mean (n = 3, 10 cells analyzed per sample). **(E)** Confirmation that measured ratios are not related to fluorescence intensity in (D). Dots represent individual cells. (**F**) Representative 405/488 nm ratio image of a NEM-conserved PFA-fixed H1975 tumor specimen expressing mito-roGFP2-Orp1. (**G**) Enlarged views allow to discriminate roGFP2 redox states in individual cells (top panels: 405/488 nm ratio images; bottom panels: nuclei (blue) and GFP fluorescence (green)), representative of regions with (i) mostly reduced (ii) mixed and (iii) fully oxidized mito-roGFP2-Orp1. (**H**) Ratio images of PFA-fixed cryosections with and without NEM pretreatment. 'Ox' and 'Red' indicate fully oxidized and reduced regions, respectively. Intratumoral 'Ox' regions remain oxidized regardless of NEM treatment. In contrast, ‘Red’ regions exhibit artificial oxidation in the absence, but not in the presence, of NEM treatment. Bar: 50 µm. (**I**) Degree of probe oxidation (based on five sections derived from three different tumors) in regions ‘Ox’ and ‘Red’ corresponding to (**H**). Boxes: lower/upper quartile; whiskers: 5^{th}/95^{th} percentile.

Fig. 3. In situ visualization of the conserved in vivo roGFP2-Orp1 redox state on liver tissue sections. (**A**) Representative 405/488 nm ratio image of liver sections from mice adenovirally transduced with mito-roGFP2-Orp1. Top panels: 405/488 nm ratio images; bottom panels: nuclei (blue) plus GFP (green). Inset: enlarged view of highly oxidized cells.

Mice were injected with either PBS, TNFα, LPS or ConA. **(B)** Dot plot representing the degree of probe oxidation (n=60 cells, from 2 animals, 30 cells per animal/treatment). Bar: Mean. (**C**) Representative images of liver sections from mice adenovirally transduced with mito-roGFP2-Orp1 and treated with TNFα, showing the 405/488 nm ratio (left panel), CD11b antibody (right panel) (n= 3). Bar: 30 µm. (**D**) Enlarged view shows the roGFP2 redox state in individual cells from different regions: (i) CD11b positive and (ii) CD11b negative.

Fig. 4. In situ visualization of mito-Grx1-roGFP2 in brain sections from transgenic mice. (**A**) Representative 405/488 nm ratio image of the coronal hippocampus from *thy1*-mito-Grx1-roGFP2 transgenic mice. The granule cell layer of the dentate gyrus (DG), and pyramidal cell regions CA1-3 are indicated. Scale bar: 500 µm. (**B**) Representative ratio (top panels) and fluorescence images (bottom panels, GFP (green) plus Nuclei (blue)) of different hippocampal regions (GrDG, CA1, and CA2/3). Bar: 50 µm. (**C**) Dot plot representing the degree of probe oxidation in different cells (n = 90 cells/region, 3 animals, 30 cells/region). Different colors represent different mice. Statistical analysis was conducted by paired Student-test. GrDG vs Py/CA1: *p < 0.05 , GrDG vs Py/CA2&3 and *p < 0.05, Py/CA1 vs Py/CA2&3 p=0.4072.

Fig. 5. Histological redox imaging using mito-roGFP2-Orp1 transgenic mice. (**A**) NEM prevents artificial probe oxidation in tissue sections from mito-roGFP2-Orp1-transgenic mice. Representative ratio images showing PFA-fixed choroid plexus endothelial cells prepared with or without prior NEM treatment. Scale bar: 50 µm. The inset shows an enlargement. (**B**) Degree of probe oxidation (n = 3). Boxes: lower/upper quartile; whiskers: 5th/95th percentile. (**C**) Normalized ratio of liver sections derived from mito-roGFP2-Orp1 treated with different combinations of DA, DTT and NEM as specified on the graph. Arrow means “followed by”. NEM-pretreated (50 mM) liver cryosections were treated for 10 minutes with the strong thiol-oxidizing agent diamide (DA) (2 mM) prior to fixation with 4% PFA. NEM was found to prevent oxidation by DA. (**D**) Representative ratio image of a mito-roGFP2-Orp1-transgenic E12.5 embryo conserved with NEM before PFA fixation (n = 9). The inset shows the embryonic liver where several globular regions of increased probe oxidation are detected. (**E**) Representative 405/488 nm ratio images of mito-roGFP2-Orp1-transgenic gastrocnemius/soleus muscles after 24 h of feeding (FED) or fasting (FAST) (n=7-8 animals per group). Muscle tissue was dissected and immediately snap-frozen. Sections were treated

with or without NEM prior to fixation with 4% PFA. (**F**) Degree of probe oxidation and statistical analysis of fasting-related redox changes. Student's t-test followed by Welch's correction test: **p < 0.01; Fold changes after log–transformation using Student's t-test: p = 0.0046: FAST NEM vs FED NEM. (**G**) Representative fluorescence and ratio images of longitudinal and cross-sectional muscle sections. Mice lacking sensor expression (left column) were used as autofluorescence controls and background was calculated for each wavelength. Cryosections were treated with NEM prior to fixation and imaged by excitation at 405 nm and 488 nm to obtain the ratio images. Bar: 100 µm. n= 3-4 animals. (**H**) Degree of probe oxidation in longitudinal sections (left panel) and cross-sections (right panel). Error bars represent S.E.M. Boxes: lower/upper quartile; whiskers: 5^{th}/95^{th} percentile. Student's t-test: **p < 0.001; * p < 0.05.

REFERENCES AND NOTES

1. M. Schieber, N. S. Chandel, ROS function in redox signaling and oxidative stress. *Curr Biol* **24**, R453-462 (2014); published online EpubMay 19 (10.1016/j.cub.2014.03.034).
2. M. Ristow, Unraveling the truth about antioxidants: mitohormesis explains ROS-induced health benefits. *Nature medicine* **20**, 709-711 (2014); published online EpubJul (10.1038/nm.3624).
3. J. Yun, T. Finkel, Mitohormesis. *Cell Metab* **19**, 757-766 (2014); published online EpubMay 6 (10.1016/j.cmet.2014.01.011).
4. M. Gutscher, M. C. Sobotta, G. H. Wabnitz, S. Ballikaya, A. J. Meyer, Y. Samstag, T. P. Dick, Proximity-based protein thiol oxidation by H2O2-scavenging peroxidases. *The Journal of biological chemistry* **284**, 31532-31540 (2009); published online EpubNov 13 (10.1074/jbc.M109.059246).
5. V. V. Belousov, A. F. Fradkov, K. A. Lukyanov, D. B. Staroverov, K. S. Shakhbazov, A. V. Terskikh, S. Lukyanov, Genetically encoded fluorescent indicator for intracellular hydrogen peroxide. *Nat Methods* **3**, 281-286 (2006); published online EpubApr (10.1038/nmeth866).
6. M. Gutscher, A. L. Pauleau, L. Marty, T. Brach, G. H. Wabnitz, Y. Samstag, A. J. Meyer, T. P. Dick, Real-time imaging of the intracellular glutathione redox potential. *Nat Methods* **5**, 553-559 (2008); published online EpubJun (10.1038/nmeth.1212).
7. S. C. Albrecht, A. G. Barata, J. Grosshans, A. A. Teleman, T. P. Dick, In vivo mapping of hydrogen peroxide and oxidized glutathione reveals chemical and regional specificity of redox homeostasis. *Cell Metab* **14**, 819-829 (2011); published online EpubDec 7 (10.1016/j.cmet.2011.10.010).
8. M. O. Breckwoldt, F. M. Pfister, P. M. Bradley, P. Marinkovic, P. R. Williams, M. S. Brill, B. Plomer, A. Schmalz, D. K. St Clair, R. Naumann, O. Griesbeck, M. Schwarzlander, L. Godinho, F. M. Bareyre, T. P. Dick, M. Kerschensteiner, T. Misgeld, Multiparametric optical analysis of mitochondrial redox signals during neuronal physiology and pathology in vivo. *Nature medicine* **20**, 555-560 (2014); published online EpubMay (10.1038/nm.3520).
9. B. Morgan, D. Ezerina, T. N. Amoako, J. Riemer, M. Seedorf, T. P. Dick, Multiple glutathione disulfide removal pathways mediate cytosolic redox homeostasis. *Nature chemical biology* **9**, 119-125 (2013); published online EpubFeb (10.1038/nchembio.1142).
10. M. Schwarzlander, T. P. Dick, A. J. Meye, B. Morgan, Dissecting Redox Biology using Fluorescent Protein Sensors. *Antioxid Redox Signal*, (2015); published online EpubApr 13 (10.1089/ars.2015.6266).
11. D. Knoefler, M. Thamsen, M. Koniczek, N. J. Niemuth, A. K. Diederich, U. Jakob, Quantitative in vivo redox sensors uncover oxidative stress as an early event in life. *Molecular cell* **47**, 767-776 (2012); published online EpubSep 14 (10.1016/j.molcel.2012.06.016).
12. P. Niethammer, C. Grabher, A. T. Look, T. J. Mitchison, A tissue-scale gradient of hydrogen peroxide mediates rapid wound detection in zebrafish. *Nature* **459**, 996-999 (2009); published online EpubJun 18 (10.1038/nature08119).
13. D. Walter, A. Lier, A. Geiselhart, F. B. Thalheimer, S. Huntscha, M. C. Sobotta, B. Moehrle, D. Brocks, I. Bayindir, P. Kaschutnig, K. Muedder, C. Klein, A. Jauch, T. Schroeder, H. Geiger, T. P. Dick, T. Holland-Letz, P. Schmezer, S. W. Lane, M. A. Rieger, M. A. Essers, D. A. Williams, A. Trumpp, M. D. Milsom, Exit from dormancy provokes DNA-damage-induced attrition in haematopoietic stem cells. *Nature* **520**, 549-552 (2015); published online EpubApr 23 (10.1038/nature14131).
14. E. Owusu-Ansah, U. Banerjee, Reactive oxygen species prime Drosophila haematopoietic progenitors for differentiation. *Nature* **461**, 537-541 (2009); published online EpubSep 24 (10.1038/nature08313).

15. H. Bai, W. Zhang, X. J. Qin, T. Zhang, H. Wu, J. Z. Liu, C. X. Hai, Hydrogen peroxide modulates the proliferation/quiescence switch in the liver during embryonic development and posthepatectomy regeneration. *Antioxid Redox Signal* **22**, 921-937 (2015); published online EpubApr 10 (10.1089/ars.2014.5960).
16. H. P. Guan, J. L. Goldstein, M. S. Brown, G. Liang, Accelerated fatty acid oxidation in muscle averts fasting-induced hepatic steatosis in SJL/J mice. *The Journal of biological chemistry* **284**, 24644-24652 (2009); published online EpubSep 4 (10.1074/jbc.M109.034397).
17. M. Rahman, M. Mofarrahi, A. S. Kristof, B. Nkengfac, S. Harel, S. N. Hussain, Reactive oxygen species regulation of autophagy in skeletal muscles. *Antioxid Redox Signal* **20**, 443-459 (2014); published online EpubJan 20 (10.1089/ars.2013.5410).
18. A. J. Meyer, T. P. Dick, Fluorescent protein-based redox probes. *Antioxid Redox Signal* **13**, 621-650 (2010); published online EpubSep 1 (10.1089/ars.2009.2948).
19. M. Schwarzlander, S. Wagner, Y. G. Ermakova, V. V. Belousov, R. Radi, J. S. Beckman, G. R. Buettner, N. Demaurex, M. R. Duchen, H. J. Forman, M. D. Fricker, D. Gems, A. P. Halestrap, B. Halliwell, U. Jakob, I. G. Johnston, N. S. Jones, D. C. Logan, B. Morgan, F. L. Muller, D. G. Nicholls, S. J. Remington, P. T. Schumacker, C. C. Winterbourn, L. J. Sweetlove, A. J. Meyer, T. P. Dick, M. P. Murphy, The 'mitoflash' probe cpYFP does not respond to superoxide. *Nature* **514**, E12-14 (2014); published online EpubOct 23 (10.1038/nature13858).
20. L. P. Roma, J. Duprez, H. K. Takahashi, P. Gilon, A. Wiederkehr, J. C. Jonas, Dynamic measurements of mitochondrial hydrogen peroxide concentration and glutathione redox state in rat pancreatic beta-cells using ratiometric fluorescent proteins: confounding effects of pH with HyPer but not roGFP1. *The Biochemical journal* **441**, 971-978 (2012); published online EpubFeb 1 (10.1042/BJ20111770).
21. J. Weller, K. M. Kizina, K. Can, G. Bao, M. Muller, Response properties of the genetically encoded optical H2O2 sensor HyPer. *Free radical biology & medicine* **76**, 227-241 (2014); published online EpubNov (10.1016/j.freeradbiomed.2014.07.045).
22. D. Ezerina, B. Morgan, T. P. Dick, Imaging dynamic redox processes with genetically encoded probes. *J Mol Cell Cardiol* **73**, 43-49 (2014); published online EpubAug (10.1016/j.yjmcc.2013.12.023).
23. M. C. Sobotta, A. G. Barata, U. Schmidt, S. Mueller, G. Millonig, T. P. Dick, Exposing cells to H2O2: a quantitative comparison between continuous low-dose and one-time high-dose treatments. *Free radical biology & medicine* **60**, 325-335 (2013); published online EpubJul (10.1016/j.freeradbiomed.2013.02.017).
24. M. C. Sobotta, W. Liou, S. Stocker, D. Talwar, M. Oehler, T. Ruppert, A. N. Scharf, T. P. Dick, Peroxiredoxin-2 and STAT3 form a redox relay for H2O2 signaling. *Nature chemical biology* **11**, 64-70 (2015); published online EpubJan (10.1038/nchembio.1695).
25. D. Trachootham, J. Alexandre, P. Huang, Targeting cancer cells by ROS-mediated mechanisms: a radical therapeutic approach? *Nat Rev Drug Discov* **8**, 579-591 (2009); published online EpubJul (10.1038/nrd2803).
26. V. I. Sayin, M. X. Ibrahim, E. Larsson, J. A. Nilsson, P. Lindahl, M. O. Bergo, Antioxidants accelerate lung cancer progression in mice. *Sci Transl Med* **6**, 221ra215 (2014); published online EpubJan 29 (10.1126/scitranslmed.3007653).
27. K. Le Gal, M. X. Ibrahim, C. Wiel, V. I. Sayin, M. K. Akula, C. Karlsson, M. G. Dalin, L. M. Akyurek, P. Lindahl, J. Nilsson, M. O. Bergo, Antioxidants can increase melanoma metastasis in mice. *Sci Transl Med* **7**, 308re308 (2015); published online EpubOct 7 (10.1126/scitranslmed.aad3740).
28. E. Piskounova, M. Agathocleous, M. M. Murphy, Z. Hu, S. E. Huddlestun, Z. Zhao, A. M. Leitch, T. M. Johnson, R. J. DeBerardinis, S. J. Morrison, Oxidative stress inhibits distant metastasis by human melanoma cells. *Nature* **527**, 186-191 (2015); published online EpubNov 12 (10.1038/nature15726).

29. T. C. Becker, R. J. Noel, W. S. Coats, A. M. Gomez-Foix, T. Alam, R. D. Gerard, C. B. Newgard, Use of recombinant adenovirus for metabolic engineering of mammalian cells. *Methods in cell biology* **43 Pt A**, 161-189 (1994).
30. P. Soriano, Generalized lacZ expression with the ROSA26 Cre reporter strain. *Nature genetics* **21**, 70-71 (1999); published online EpubJan (10.1038/5007).
31. S. J. Pettitt, Q. Liang, X. Y. Rairdan, J. L. Moran, H. M. Prosser, D. R. Beier, K. C. Lloyd, A. Bradley, W. C. Skarnes, Agouti C57BL/6N embryonic stem cells for mouse genetic resources. *Nat Methods* **6**, 493-495 (2009); published online EpubJul (10.1038/nmeth.1342).
32. B. Morgan, M. C. Sobotta, T. P. Dick, Measuring E(GSH) and H2O2 with roGFP2-based redox probes. *Free radical biology & medicine* **51**, 1943-1951 (2011); published online EpubDec 1 (10.1016/j.freeradbiomed.2011.08.035).
33. A. G. Barata, T. P. Dick, In vivo imaging of H2O2 production in Drosophila. *Methods in enzymology* **526**, 61-82 (2013)10.1016/B978-0-12-405883-5.00004-1).

Acknowledgements: We thank Dr. Felix Bestvater and Dr. Manuela Brom for microscopy support, Dr. Marc Schmidt-Supprian (Technical University Munich) for the ROSA26 targeting construct, Dr. Ulrich Kloz and Dr. Frank van der Hoeven for ES cell microinjections, Anja Reimann for adenovirus preparations, Dr. Thomas Hielscher for help with statistics, Andrea Pohl-Arnold, Brigitte Steinbauer, Gabriele Kuntz, Annika Zota and Yvonne Feuchter for technical assistance. **Funding:** T.P.D. acknowledges funding by the DFG (SFB1036, SFB938 and SPP1710) and the BMBF (LungSysII). S.H. is supported by the Helmholtz Cross-Program topic "Metabolic Dysfunction" and the "ICEMED" alliance. T.M. was supported by the DFG (EXC 114, EXC 1010, SFB 870 and SPP 1710). Y.F. has been supported by the DKFZ postdoc fellowship program and the Japan Society for the Promotion of Science (JSPS). L.P.R. has been supported by a postdoctoral fellowship from the Sao Paulo Research Foundation (FAPESP) and CNPq (Conselho nacional de Pesquisa) Universal MCTI/ CNPq n° 14/2012 and by the DKFZ visiting scientist program. M.C.S. has been supported by a PhD stipend from the Boehringer Ingelheim Fonds. M.O.B. acknowledges support by a physician-scientist fellowship of the Medical Faculty, University of Heidelberg. **Author contributions:** Y.F. and L.P.R. performed experiments and analyzed data; T.P.D., M.C.S., and Y.F. designed and generated R26/mito-roGFP2-Orp1 mice; M.K., M.O.B., T.M. and T.P.D. generated and characterized *Thy1*-mito-Grx1-roGFP2 mice; K.M.D. designed and performed tumor xenograft experiments; Y.F., M.B.D. and S.H. designed and performed adenoviral gene transfer and liver inflammation experiments; A.J.R. coordinated mouse starvation experiments; Y.F. and T.P.D conceived the project and wrote the manuscript. **Competing interests:** The authors declare no competing financial interests.

Figure 1

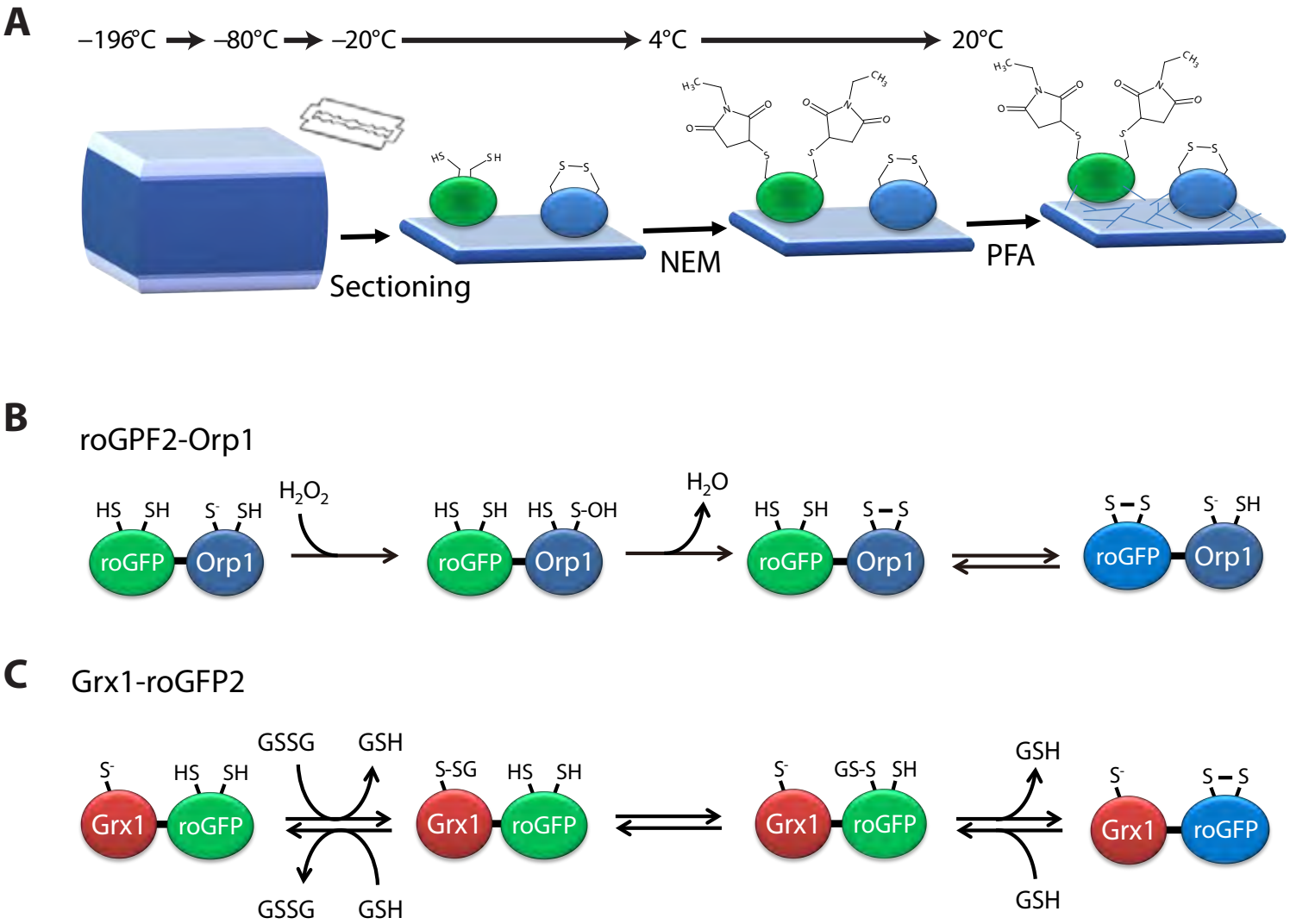
A
–196°C
–80°C
–20°C
4°C
20°C
Sectioning
NEM
PFA
B
roGPF2-Orp1
HS SH
S⁻ SH
roGFP
Orp1
H2O2
HS SH
HS S-OH
H2O
HS SH
S – S
S – S
S⁻ SH
C
Grx1-roGFP2
S⁻
HS SH
Grx1
roGFP
GSSG
GSH
S-SG
HS SH
GS-S SH
GSH
S⁻
S – S

Figure 2

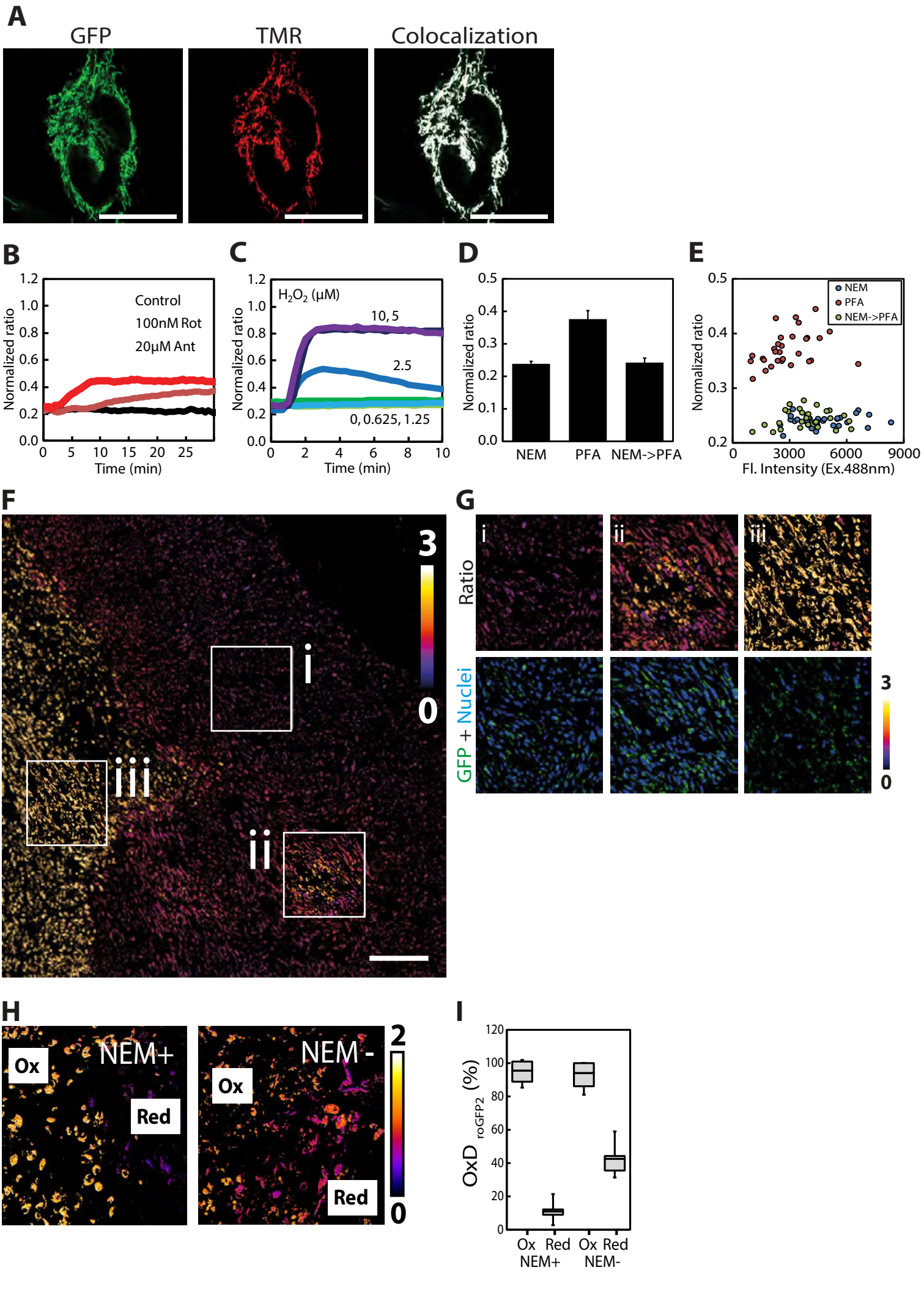
A
GFP
TMR
Colocalization
B
Normalized ratio
Control
100nM Rot
20μM Ant
Time (min)
C
H_2O_2 (μM)
10, 5
2.5
0, 0.625, 1.25
Normalized ratio
Time (min)
D
Normalized ratio
NEM
PFA
NEM->PFA
E
NEM
PFA
NEM->PFA
Normalized ratio
Fl. Intensity (Ex.488nm)
F
3
0
i
ii
iii
G
Ratio
GFP + Nuclei
i
ii
iii
3
0
H
Ox
NEM+
Red
Ox
NEM -
Red
2
0
I
OxD roGFP2 (%)
Ox
Red
Ox
Red
NEM+
NEM-

Figure 3

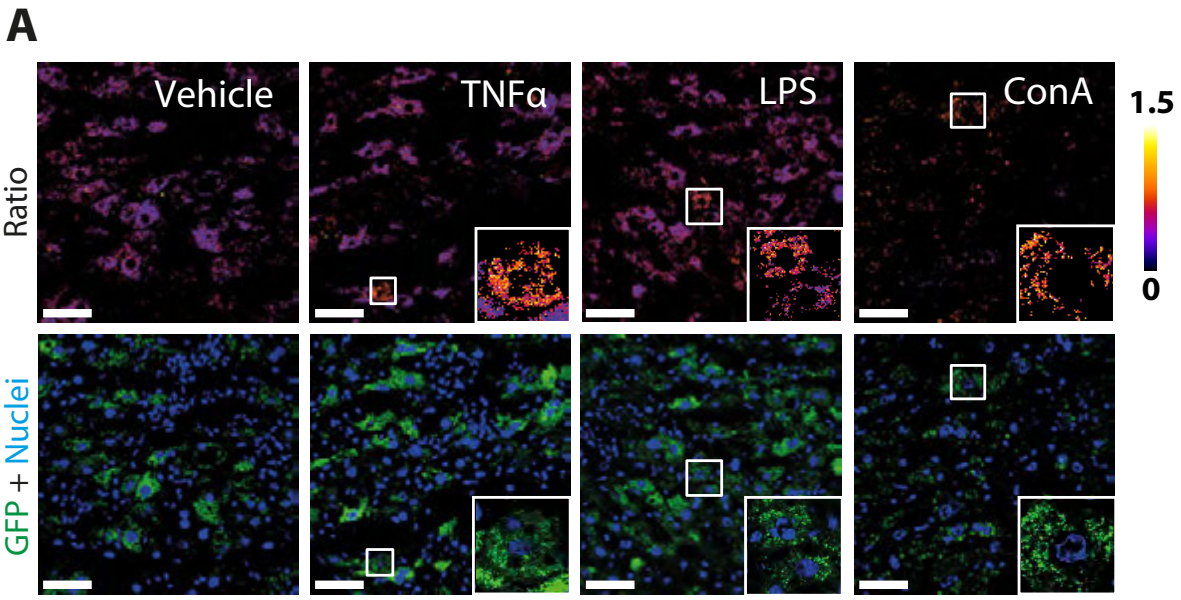
A
Vehicle
TNFα
LPS
ConA
Ratio
GFP + Nuclei
1.5
0

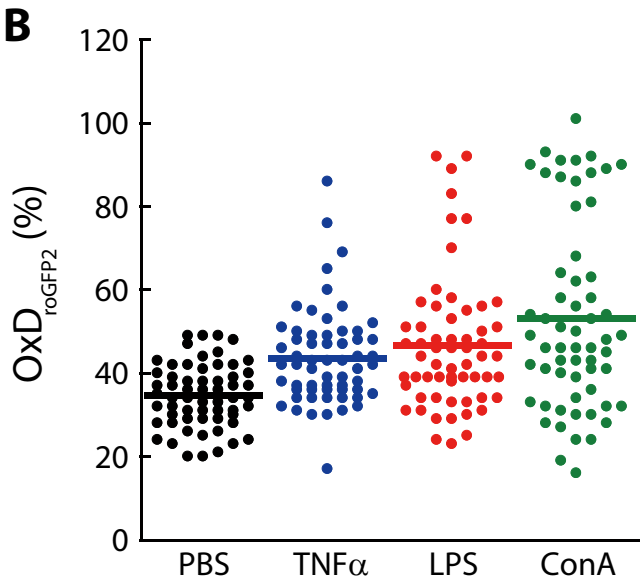
B
120
100
80
60
40
20
0
OxD roGFP2 (%)
PBS
TNFα
LPS
ConA

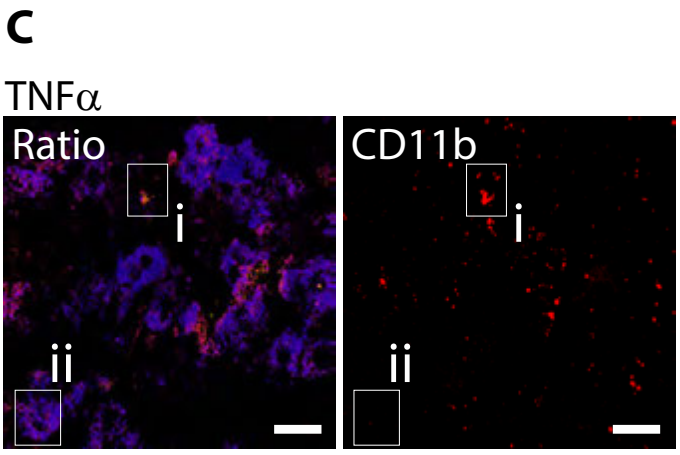
C
TNFα
Ratio
CD11b
i
ii

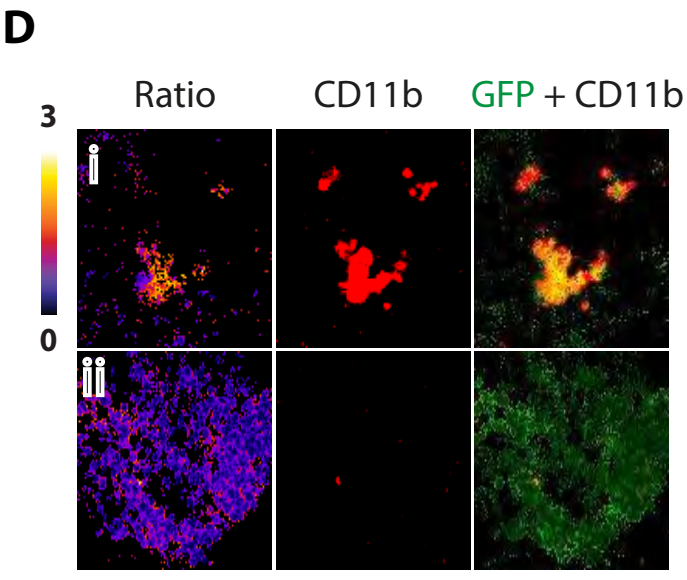
D
Ratio
CD11b
GFP + CD11b
3
0
i
ii

Figure 4

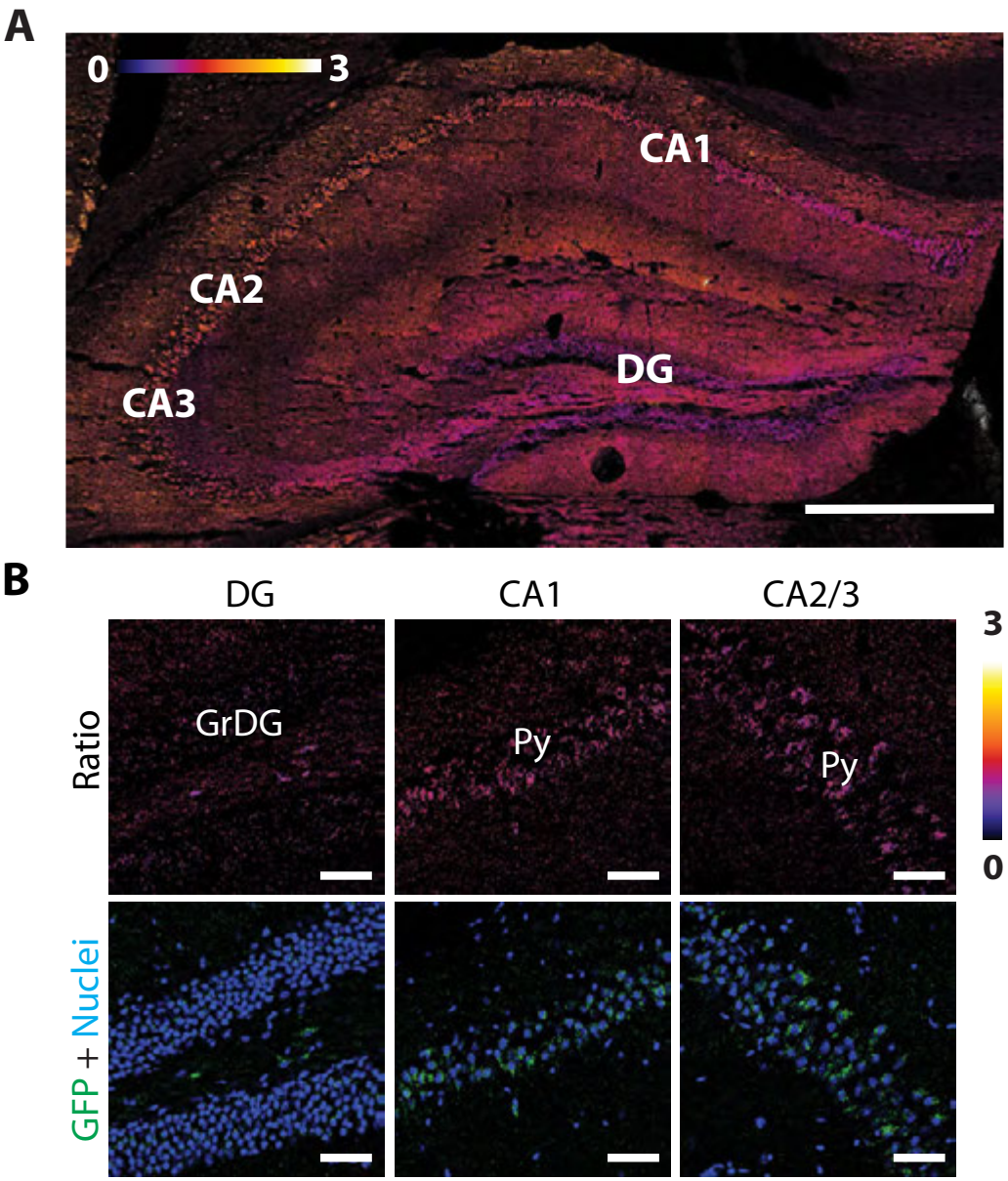
A
0
3
CA1
CA2
DG
CA3
B
DG
CA1
CA2/3
Ratio
GrDG
Py
Py
3
0
GFP + Nuclei
C
50
40
30
20
10
0
OxD roGFP2 (%)
**
*
GrDG
Py/CA1
Py/CA2&3

Figure 5

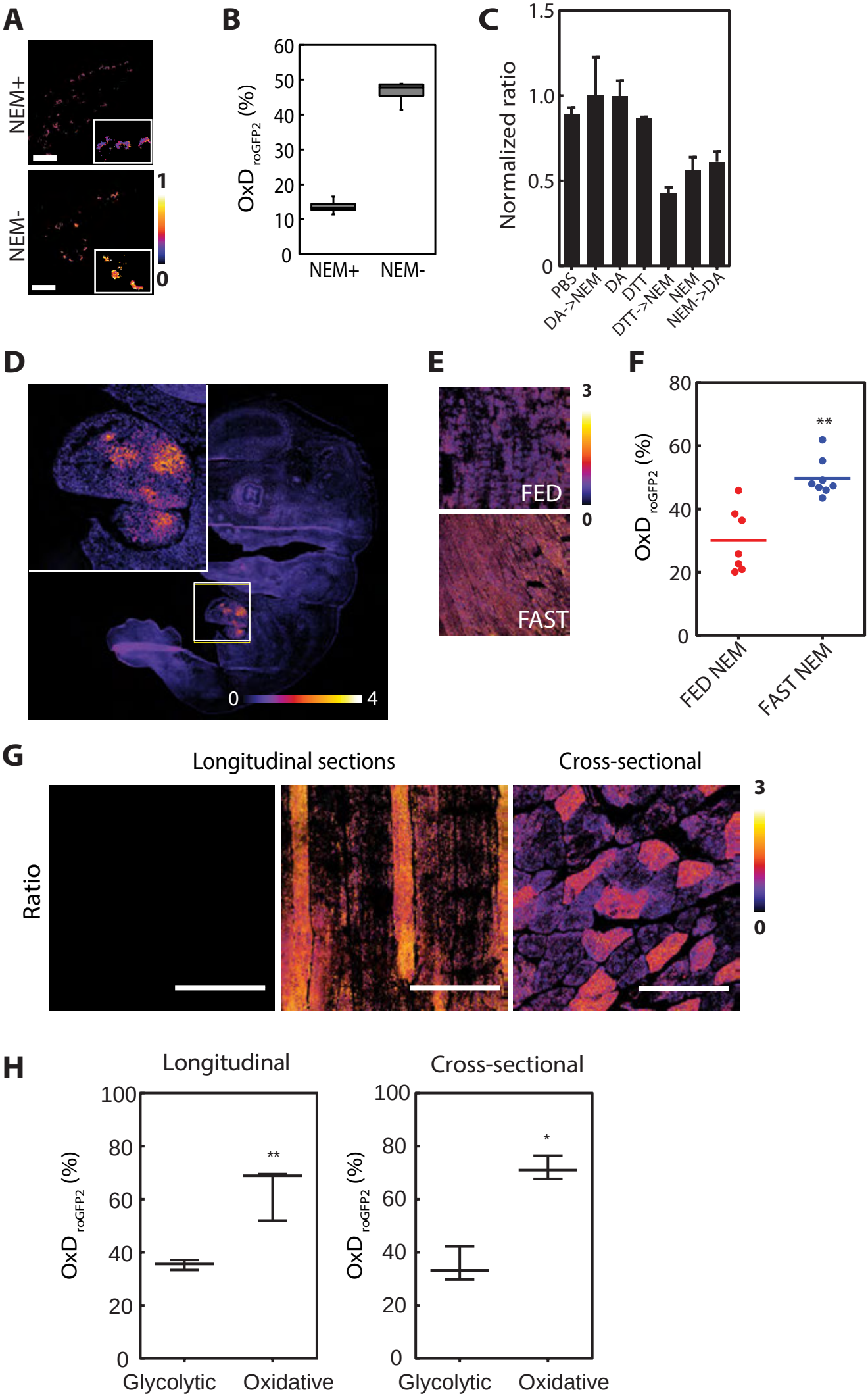
A
NEM+
NEM-
1
0
B
OxD roGFP2 (%)
60
50
40
30
20
10
0
NEM+
NEM-
C
Normalized ratio
1.5
1.0
0.5
0
PBS
DA->NEM
DA
DTT
DTT->NEM
NEM
NEM->DA
D
0
4
E
FED
FAST
3
0
F
OxD roGFP2 (%)
80
60
40
20
0
**
FED NEM
FAST NEM
G
Longitudinal sections
Cross-sectional
Ratio
3
0
H
Longitudinal
Cross-sectional
OxD roGFP2 (%)
100
80
60
40
20
0
**
*
Glycolytic
Oxidative

Supplementary Materials for

Mouse redox histology using genetically encoded probes

Yuuta Fujikawa, Leticia P. Roma, Mirko C. Sobotta, Adam J. Rose, Mauricio Berriel Diaz, Giuseppe Locatelli, Michael O. Breckwoldt, Thomas Misgeld, Martin Kerschensteiner, Stephan Herzig, Karin Müller-Decker & Tobias P. Dick*

*Corresponding author, E-mail: t.dick@dkfz.de

This PDF file includes:

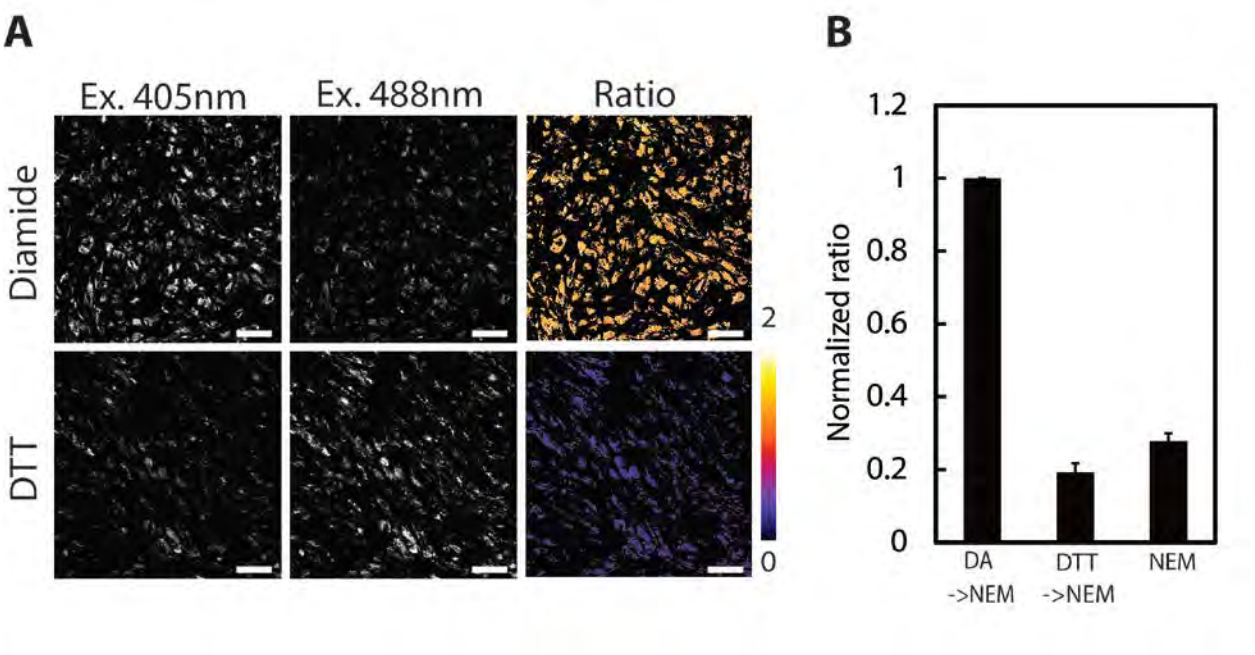

Figure S1. Responsiveness of mito-roGFP2-Orp1 within tumor tissue sections. (**A**) Representative fluorescence and ratio images. Sections subjected to 1 mM diamide (DA) (upper panels) and 20 mM DTT (lower panels) were imaged after excitation at 405 nm (left panels) and 488 nm (middle panels), to obtain ratio images (right panels). Bar: 50 µm. (**B**) Normalized ratio values of samples treated with DA or DTT or left untreated before NEM blocking. The fully oxidized state is normalized to 1. Data represent the mean ± S.E.M. (n =4).

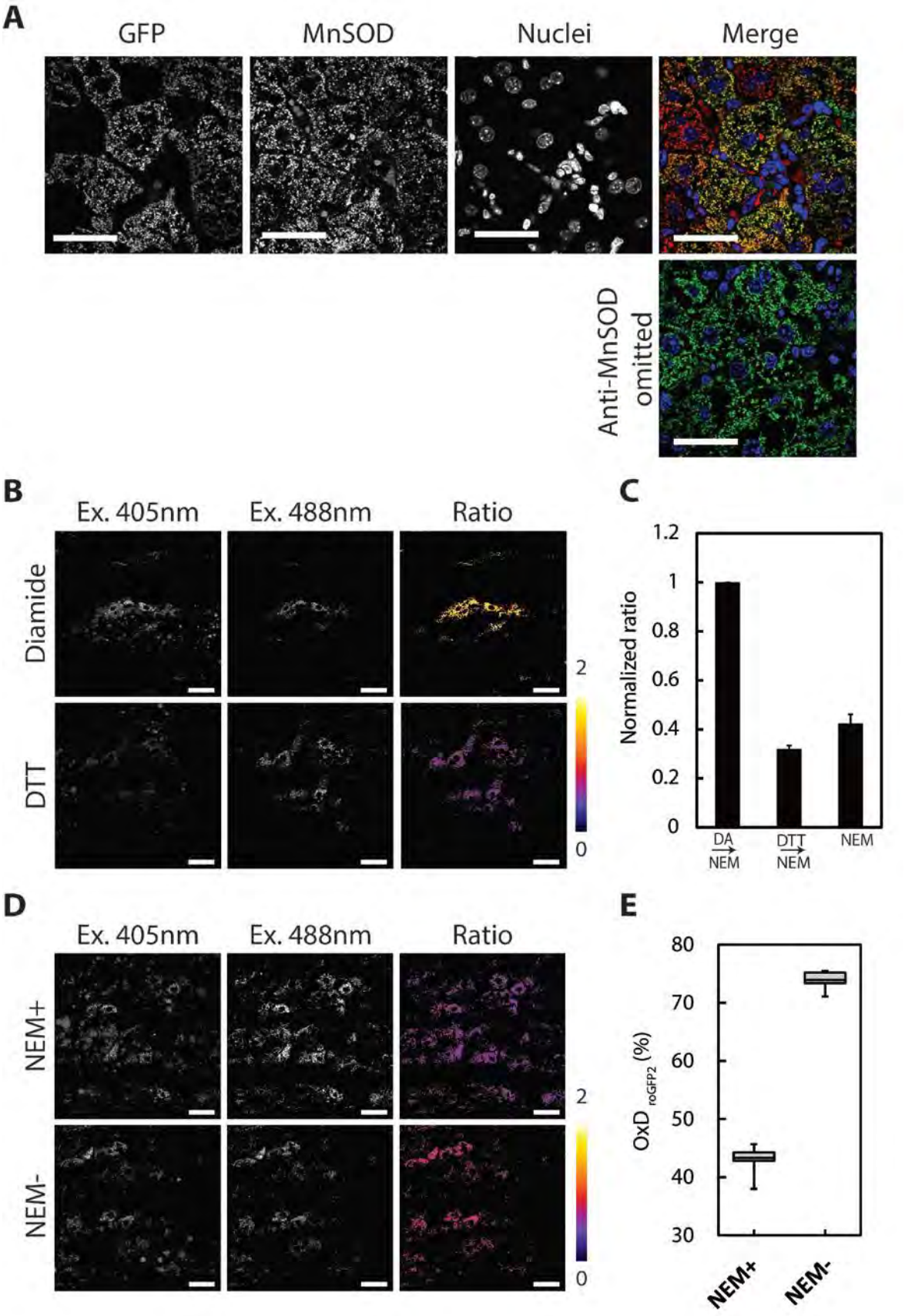
A
GFP
MnSOD
Nuclei
Merge
Anti-MnSOD omitted
B
Ex. 405nm
Ex. 488nm
Ratio
Diamide
DTT
2
0
C
Normalized ratio
1.2
1
0.8
0.6
0.4
0.2
0
DA → NEM
DTT → NEM
NEM
D
Ex. 405nm
Ex. 488nm
Ratio
NEM+
NEM-
2
0
E
OxD roGFP2 (%)
80
70
60
50
40
30
NEM+
NEM-

Figure S2. In situ characterization of the mito-roGFP2-Orp1 redox state on cryosections from adenovirally transduced liver. (**A**) Colocalization of roGFP2 and mitochondrial manganese-dependent superoxide dismutase (MnSOD). Confocal images of 50 µm fixed liver sections showing biosensor (green; direct fluorescence), MnSOD (red; indirect immunofluorescence), and ToPro-3 nuclear staining (blue). Scale bar: 40 µm. (**B**) Representative fluorescence and ratio images. Sections subjected to 1 mM diamide (DA) (top panels) and 10 mM DTT (bottom panels), imaged by excitation at 405 nm (left panels) and 488 nm (middle panels), and the corresponding ratio (right panels). (**C**) Normalized ratio values of samples treated with DA or DTT or left untreated before NEM blocking. Data represent the mean ± S.E.M. (n=4) (**D**) Fluorescence and ratio images of PFA-fixed sections with or without NEM pretreatment. (**E**) Degree of roGFP2 oxidation (n = 6, two animals, three sections per treatment). Boxes: lower/upper quartile; whiskers: 5^{th}/95^{th} percentile. Bar: 40 µm (A), 50 µm (B, D).

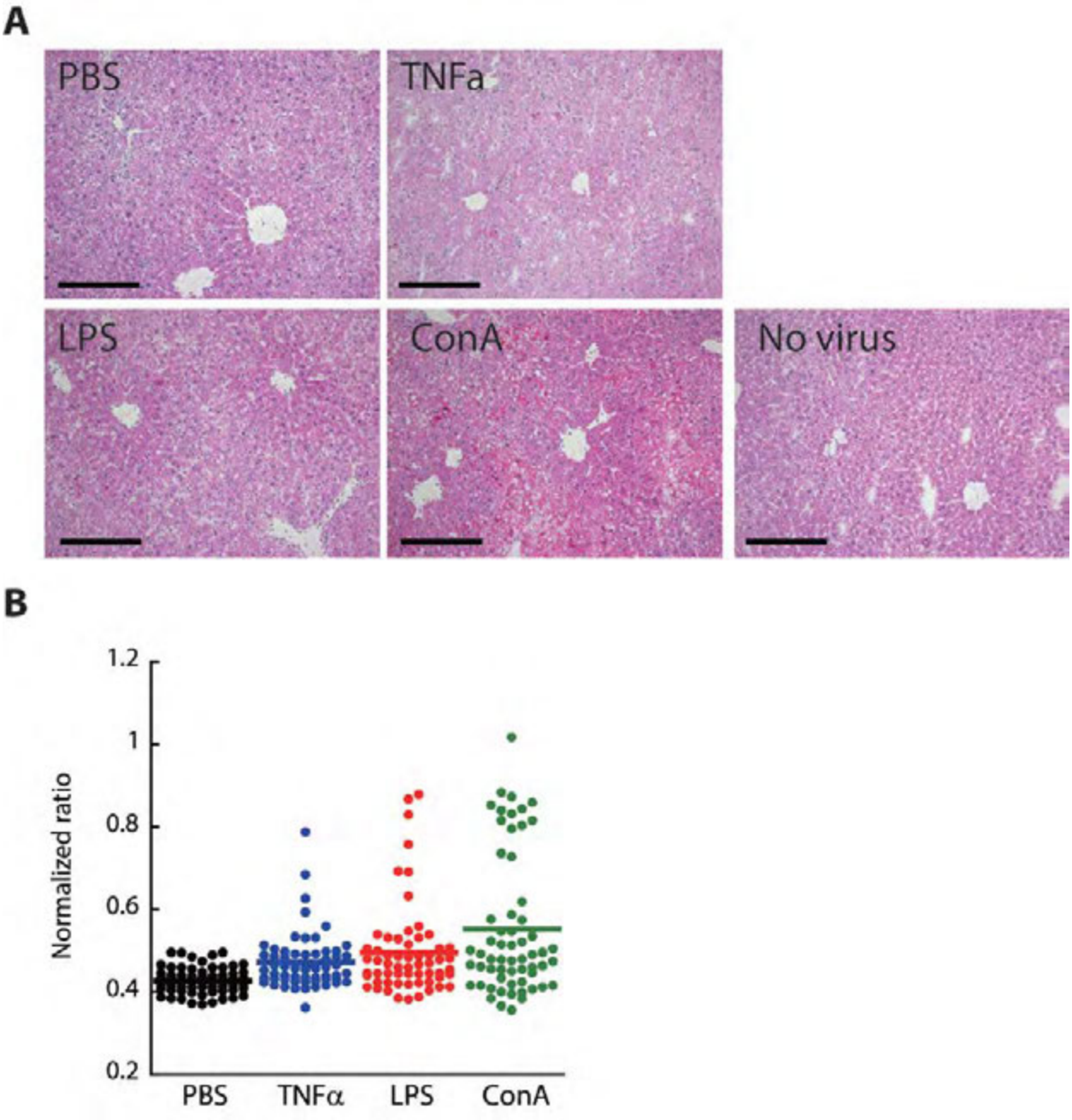

Figure S3. Inflammation-associated liver injury. (A) Representative HE-staining of liver sections from adenovirally infected mice injected with PBS, TNFα, LPS, and ConA or from a non-infected mouse. Bar: 200 µm. (**B**) Dot plots showing normalized ratio values for individual cells in liver sections from mice injected with either PBS, TNFα, LPS, and ConA (n= 2 animals, 30 cells were analyzed in each animal/ treatment). The fully oxidized state is normalized to 1.

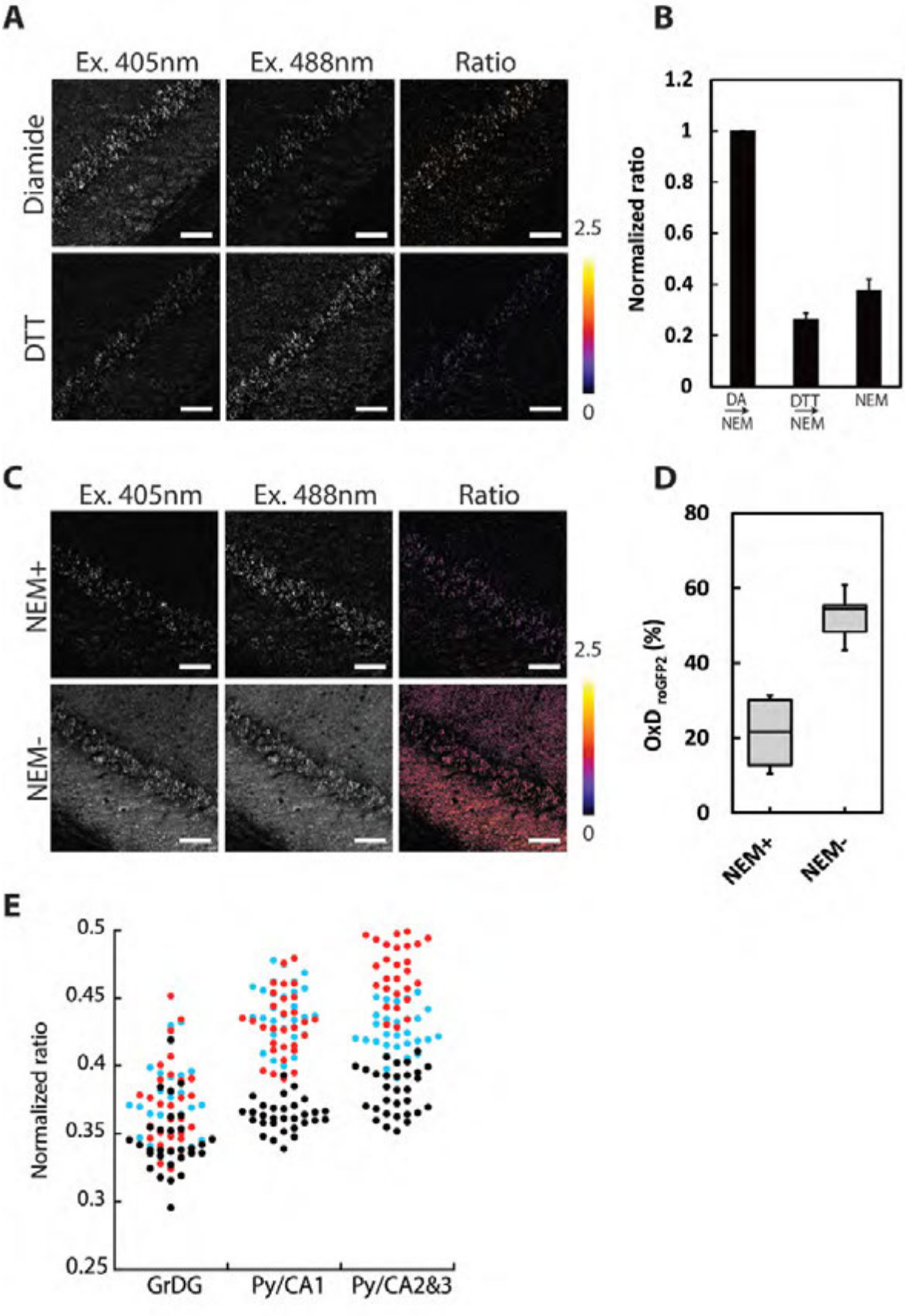
A
Ex. 405nm
Ex. 488nm
Ratio
Diamide
DTT
2.5
0
B
Normalized ratio
1.2
1
0.8
0.6
0.4
0.2
0
DA → NEM
DTT → NEM
NEM
C
Ex. 405nm
Ex. 488nm
Ratio
NEM+
NEM-
2.5
0
D
OxD roGFP2 (%)
80
60
40
20
0
NEM+
NEM-
E
Normalized ratio
0.5
0.45
0.4
0.35
0.3
0.25
GrDG
Py/CA1
Py/CA2&3

Figure S4. In situ characterization of the roGFP2 redox state on cryosections from *Thy1*-mito-Grx1-roGFP2 mice. (**A**) Representative fluorescence and ratio images (n = 5). Sections subjected to 1 mM diamide (DA) (top panels) and 10 mM DTT treatment (bottom panels) were imaged by excitation at 405 nm and 488 nm, to obtain ratio images. (**B**) Normalized ratio values of samples treated with DA or DTT or left untreated before NEM blocking. Data represent the mean ± S.E.M. (n=5). (**C**) Fluorescence and ratio images of PFA-fixed sections with or without NEM pretreatment. (**D**) Degree of roGFP2 oxidation (n = 9, two animals, three sections per animal). Boxes: lower/upper quartile; whiskers: 5^{th}/95^{th} percentile. Bar: 50 µm (A and C). (**E**) Dot plot showing normalized ratio values of individual cells in different brain regions of three different mice. Different colors represent individual mice (n= 30 cells each animal). The fully oxidized state is normalized to 1.

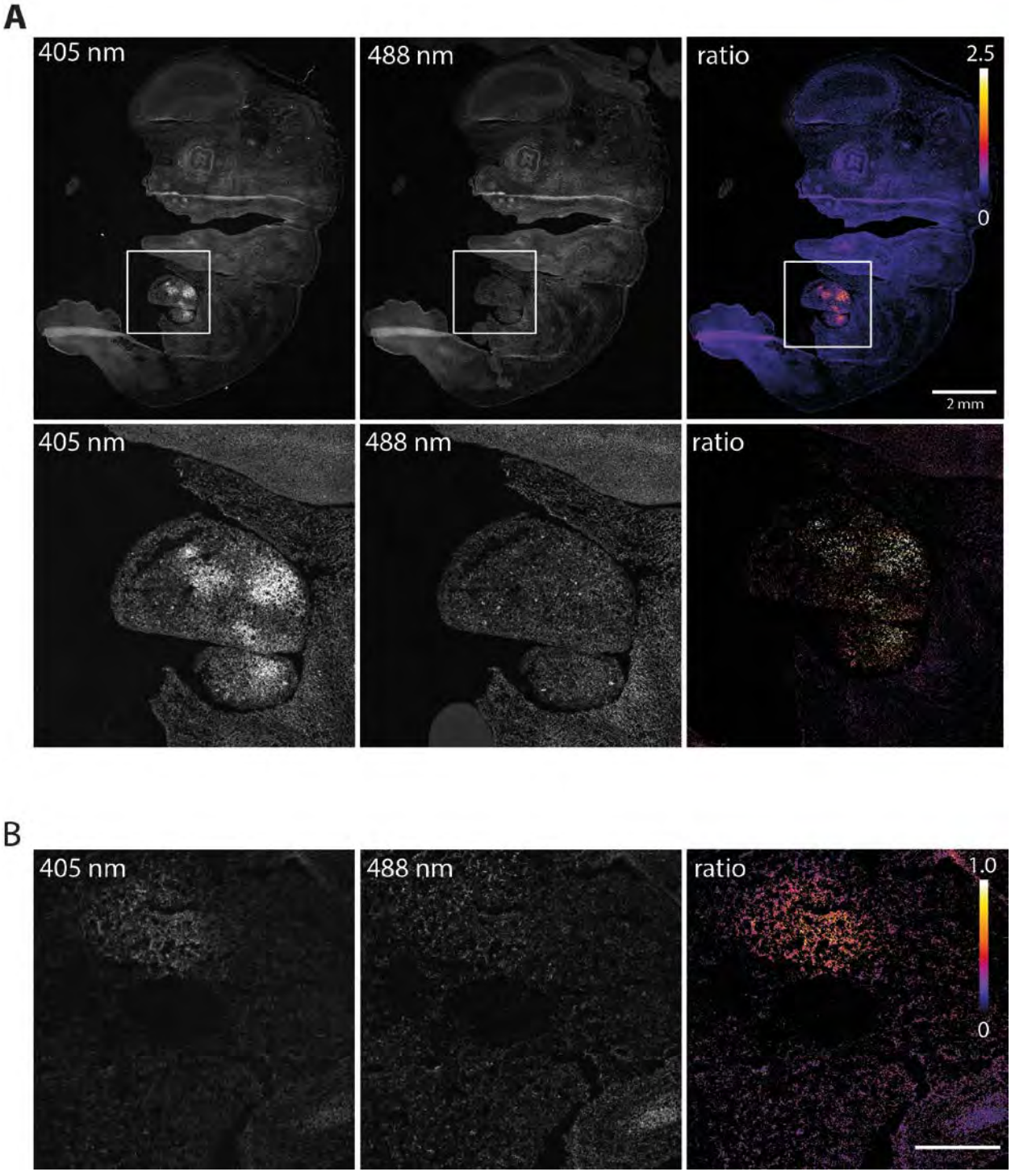
A
405 nm
488 nm
ratio
2.5
0
2 mm
405 nm
488 nm
ratio
B
405 nm
488 nm
ratio
1.0
0

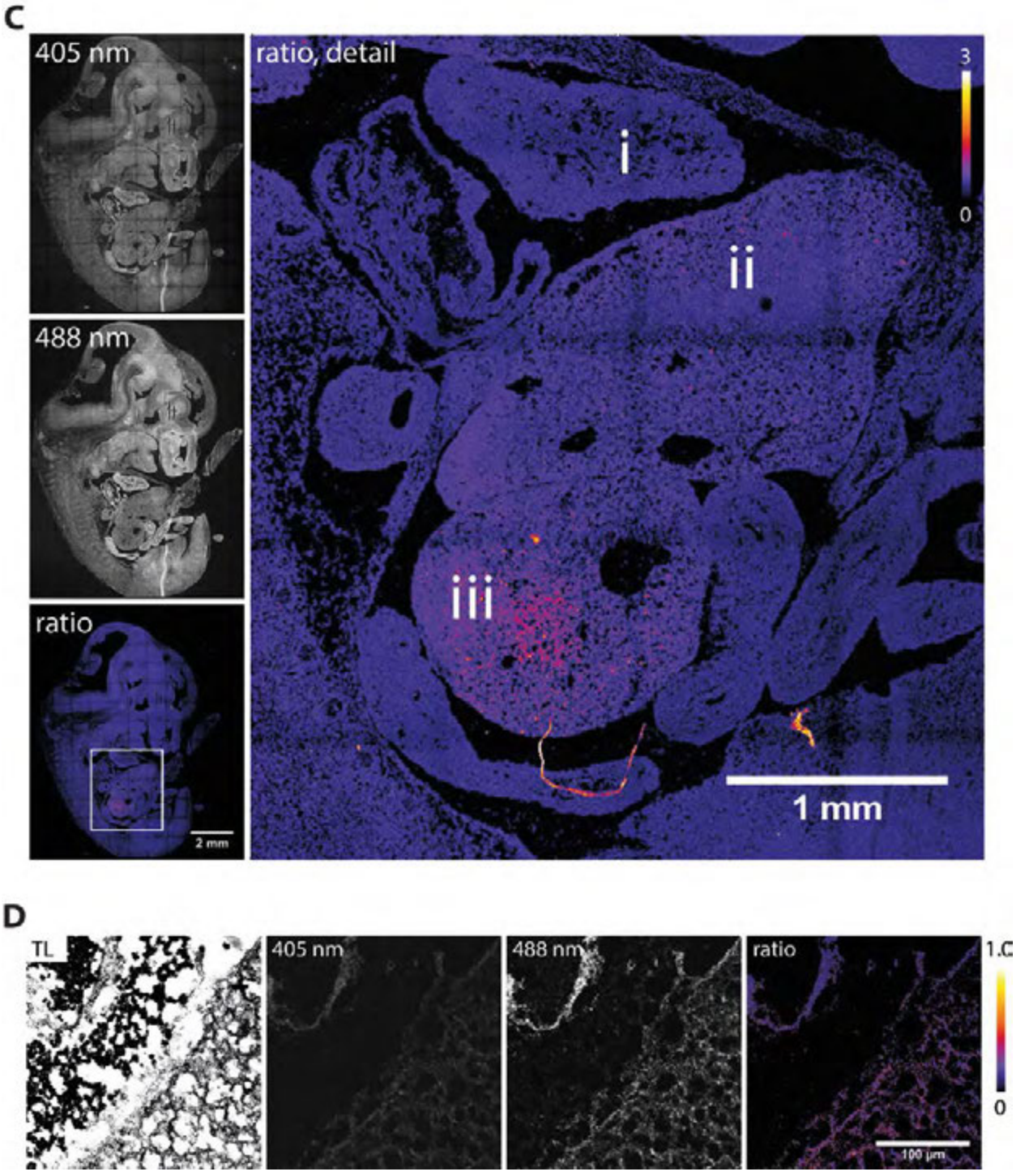
C
405 nm
488 nm
ratio
2 mm
ratio, detail
3
0
i
ii
iii
1 mm
D
TL
405 nm
488 nm
ratio
1.0
0
100 µm

Figure S5. Analysis of mito-roGFP2-Orp1-transgenic embryos. (**A-D**) Embryos dissected at gestational stage E12.5 (n = 12) were treated with NEM prior to fixation with 4% PFA plus NEM. Specimens were snap frozen and 14µm cryosections imaged by sequential excitation at 405 nm and 488 nm. (**A**) Composite images of the embryo shown in Fig. 5D. Scale bar: 2 mm. The liver region is shown at higher magnification to highlight regions of increased probe oxidation (lower panels). (**B**) Corresponding liver images from a different embryo taken with a 40x objective, again showing a globular region of increased sensor oxidation. Scale bar: 200 µm. (**C**) Composite fluorescence and ratio images of another E12.5 embryo. The enlarged inset (large panel) indicates areas (i, ii, iii) of differing probe redox status (i: heart, ratio=1.02; ii: liver, ratio=1.12: iii: liver, ratio=1.38). Scale bar: 1 mm. (**D**) Representative images of embryonic liver imaged with a 40x objective (n = 5). Maturing red blood cells (dark dots in the TL image) exhibit very low probe expression. TL: transmitted light. Scale bar: 100µm.

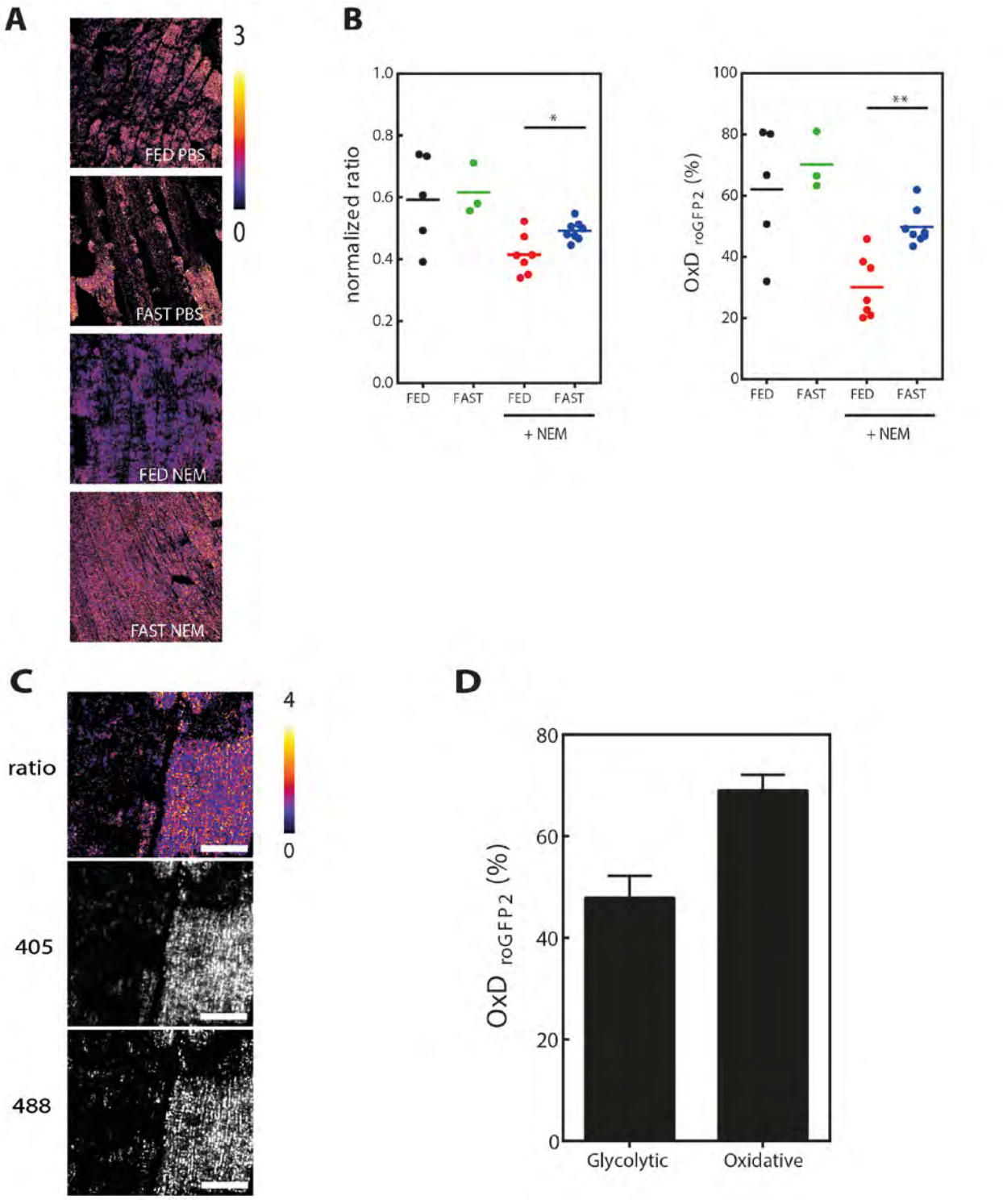
A
3
0
FED PBS
FAST PBS
FED NEM
FAST NEM
B
normalized ratio
1.0
0.8
0.6
0.4
0.2
0.0
*
FED
FAST
FED
FAST
+ NEM
OxD roGFP2 (%)
100
80
60
40
20
0
**
FED
FAST
FED
FAST
+ NEM
C
ratio
405
488
4
0
D
OxD roGFP2 (%)
80
60
40
20
0
Glycolytic
Oxidative

Figure S6. Analysis of muscle sections from mito-roGFP2-Orp1-transgenic mice. (**A**) Representative 405/488 nm ratio images of mito-roGFP2-Orp1-transgenic gastrocnemius/soleus muscles after 24 hours of feeding (FED) or fasting (FAST) (n = 7-8). Muscle tissue was dissected and immediately snap-frozen. Sections were treated with or without NEM prior to fixation with 4% PFA. (**B)** Statistical analysis of fasting-related redox changes. Left panel represents normalized ratio values. *$p<0.05$. Student's t-test with Welsch's correction. The right panel represents the corresponding degree of roGFP2 oxidation. ** $p<0.01$. Student's t-test with Welsch's correction compares FED NEM and FAST NEM. Samples not treated with NEM are only shown to demonstrate that NEM treatment prevents artificial oxidation. The fully oxidized state is normalized to 1. (**C**) Representative 405/488 nm ratio images of adjacent muscle fibers demonstrating low and high mitochondrial density. Bar: 10 µm. (**D**) Degree of mito-roGFP2-Orp1 oxidation in different fibers (based on 3-4 animals).